Fast and Slow Dynamics in a Discotic Liquid Crystal with Regions of Columnar Order and Disorder

M. R. Hansen,[1,*] X. Feng,[1] V. Macho,[1] K. Müllen,[1] H. W. Spiess,[1] and G. Floudas[2,†]

[1]*Max-Planck-Institut für Polymerforschung, D-55021 Mainz, Germany*

[2]*Department of Physics, University of Ioannina, 451 10 Ioannina, Greece and Biomedical Research Institute (BRI), Foundation for Research and Technology-Hellas (FORTH), 451 10 Ioannina, Greece*

(Received 31 March 2011; revised manuscript received 1 June 2011; published 14 December 2011)

Aromatic disk-shaped molecules tend to self-organize into a herringbone packing where the disks are inclined at angles $\pm\theta$ with respect to the axis of the column. In discotic liquid crystals this can introduce defects between stacks of limited length. In a C_3-symmetric hexa-*peri*-hexabenzocoronene, solid-state NMR, x-ray scattering, and rheology identifies such a packing with $\theta = 43°$ and stacks of about seven disks. Disordered regions containing defects fill the space in between the ordered stacks. Biaxial intra- and intercolumnar dynamics differing by eight decades are identified.

DOI: 10.1103/PhysRevLett.107.257801 PACS numbers: 61.30.Cz, 64.70.M−, 76.60.−k, 83.80.Xz

Supramolecular organization of molecules with different structural elements can generate nanostructures containing regions of order and disorder crucial for their function. Block copolymers, organic-inorganic hybrids, and even semicrystalline homopolymers are examples of such molecularly controlled systems. The characterization of such materials requires the determination of both the structure and dynamics over wide length and time scales. In fact, this area of soft matter has recently been identified as one of the challenges and opportunities in macromolecular science [1]. Here, we consider another example, namely, discotic liquid crystals (DLCs) composed of rigid disk-shaped aromatic cores and disordered alkyl substituents, that self-assemble in columnar structures. Typical examples of DLCs are triphenylene and hexa-*peri*-hexabenzocoronene (HBC) derivatives. The self-assembly is driven by favorable intermolecular interactions of the aromatic cores, causing π-π stacking, and unfavorable interactions between the cores and the alkyl chains, leading to nanophase separation [2–4]. However, as pointed out by de Gennes [5], the incommensurability of flexible aliphatic side chains and rigid aromatic cores poses a packing problem. This can lead to density fluctuations along the columns that can be described as a heterogeneous disorder composed of regions of high order interrupted by defects. Considering the potential application of DLCs as self-healing active semiconductors, the presence of defects limits the one-dimensional charge transport in accord with the Anderson theory of localization [6]. For these reasons, knowledge about structural disorder in DLCs in terms of the origin of the defects, their characteristic length, and associated dynamics is essential.

For DLCs based on HBCs a number of different dynamic processes associated with fast axial motion and collective reorganization of the disks were identified in the Col_h phase [7]. In particular, NMR methods showed that the local dynamic molecular order parameter, as probed by the C−H bond direction, is close to $S_{\mathrm{CH}} = 0.5$ consistent with an axial motion of the parallel disks around the column axis [8]. Other HBC derivatives with lower symmetry exhibit a somewhat lower order ($S_{\mathrm{CH}} = 0.45$–0.38), reflecting combined axial rotations and out-of-plane fluctuations of the disks [9].

In this Letter we address a C_3-symmetric HBC with hydrophobic and hydrophilic side chains of incommensurable lengths [10] [see Fig. 1(a)] using a multitechnique approach. This particular combination of molecule symmetry and side chains with different interactions leads to an unusually low order parameter for the HBC cores of $S_{\mathrm{CH}} \sim 0.15$ in the Col_h phase, where, remarkably, the disks maintain a columnar packing as verified by wide-angle x-ray scattering (WAXS). The question then arises as to how such a low S_{CH} can be rationalized. In principle, such low dynamic order can result from homogeneous or heterogeneous disorder as illustrated in Fig. 1(b). In both cases a number of fast intracolumnar processes [Fig. 1(c)] and slow intercolumnar processes [Fig. 1(d)] can be envisaged that are associated with defect diffusion. Elucidation of such complex behavior requires a combination of different techniques. Therefore, we employ differential scanning calorimetry (DSC), WAXS, solid-state NMR, dielectric spectroscopy (DS), and rheology. This combination allows us to develop a consistent picture of both structure and dynamics.

The investigated C_3-symmetric HBC undergoes a first order phase transition, as indicated by DSC [Fig. 2(a)], with an endothermic (exothermic) peak at 343.5 K (306.1 K) and a heat of fusion (crystallization) of 40.4 J/g (37.8 J/g). Figure 2(a) also includes the temperature dependence of the real part (ε') of the dielectric function $\varepsilon^* = \varepsilon' - i\varepsilon''$. Because of the absence of a strong dipole moment the ε' values are low, but do show

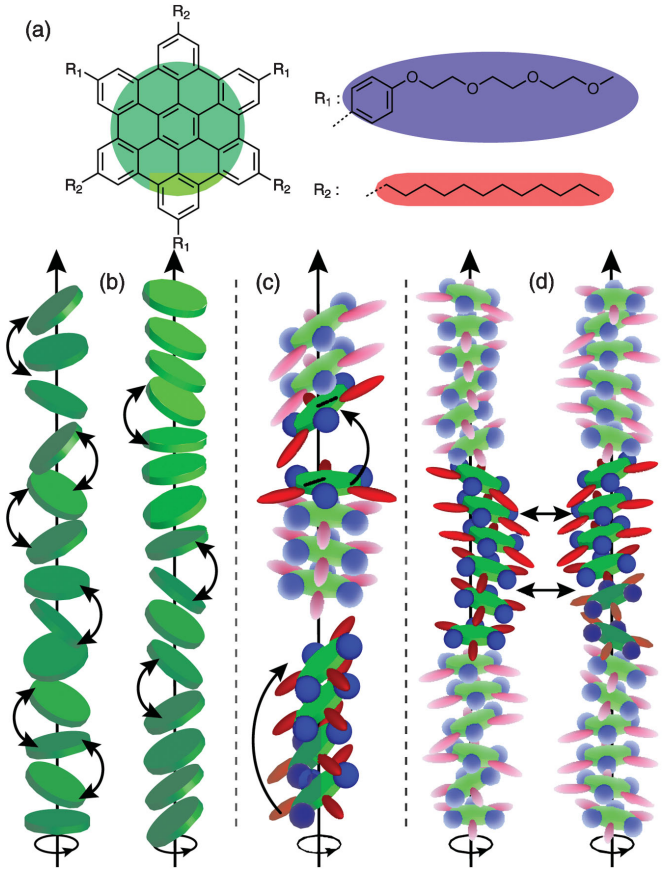

FIG. 1 (color). (a) Chemical structure of the studied DLC [10]. (b) Schematic illustration of the homogeneous (left) and heterogeneous (right) disorder along the column axis of a DLC. In both scenarios it is possible to envisage different fast and slow dynamic processes associated with defect diffusion: (c) a single molecule jumps from one molecular segment to another, or a whole group of molecules changes their orientation cooperatively, and (d) the defects can on the longer time scale occur as an intercolumnar process where segments exchange between columns.

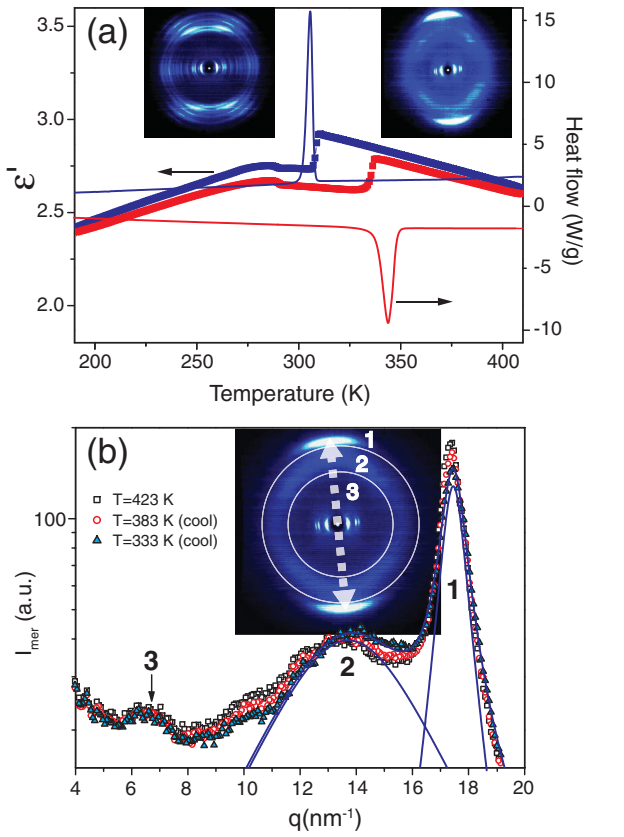

FIG. 2 (color). (a) DSC trace (thin lines) obtained during the second cooling (blue) and heating (red) with 10 K/min. Symbols refer to the dielectric permittivity measured at 2×10^5 Hz with the same rate. Insets show 2D WAXS images from an oriented fiber at 423 K (Col_h) and 303 K (C_r). (b) Intensity distribution along the meridional direction (arrow in the 2D WAXS image) at temperatures: 423 K (squares), 383 K (circles), and 333 K (triangles) obtained on cooling. Intensity maxima are labeled with 1, 2, and 3 (see text). The solid line represents a fit as a sum of two Lorentzians to the 333 K intensity profile. The patterns were recorded with a near vertical orientation of the filament axis and with the beam perpendicular to the filament.

signatures of the phase transformation by the reduction in the permittivity in the low temperature phase. Detailed 2D WAXS images obtained from extruded fibers [Fig. 2(a)] reveal that the two phases have distinctly different unit cells. The high temperature 2D WAXS image displays a set of strong meridional reflections [1 in Fig. 2(b)] associated with the typical intracolumnar periodicity of graphite (of 0.35 nm). In addition, a diffuse ring with modulated intensity is observed [2 in Fig. 2(b)]. These features were analyzed in the meridional direction as a sum of two Lorentzians, $I(q) = I_0 + \Sigma_{i=1,2} A_i w_i^2/[(q - q_i)^2 + w_i^2]$, $(q = (4\pi/\lambda)\sin(2\theta/2))$ centered around $q_1 = 17.45\,\mathrm{nm}^{-1}$ ($d_1 = 0.36$ nm) and $q_2 = 13.36\,\mathrm{nm}^{-1}$ ($d_2 = 0.47$ nm) with correlation lengths ($\xi = w^{-1}$) of 2.4 and ~0.35 nm, respectively. The first reflects the periodicity of columnar stacks of 7–8 disks. The second can be of dual origin comprising the liquidlike structure of the side chains (isotropic [11], slightly modulated [12,13], or even strongly modulated [14]) and possibly smaller regions with defected disks. Assuming that the latter predominate, the estimated volume fraction of defects amounts to 0.15. These structural features exclude the homogeneous disorder along the columns [Fig. 1(b), left]. Thus, we only consider the heterogeneous disordered case in the following.

Besides peaks 1 and 2 in the WAXS pattern, a very weak parallel line (labeled 3) is indicative of a superlattice periodicity along the columnar axis. The origin of this feature is a helical arrangement of disks within the column [12,15] with a pitch length that comprises 4 disks ($q \sim 6.8\,\mathrm{nm}^{-1}$). Furthermore, a set of strong equatorial reflections with ratios $1:3^{1/2}:4^{1/2}$ relative to the primary peak are identified, which correspond to the (10), (11), and (20) reflections of a columnar hexagonal liquid crystalline

structure (Col_h) with lattice parameter $a = 3.02$ nm. At lower temperatures the strong equatorial reflections correspond to the (10), (01), (20), (11), and (21) reflections of a monoclinic unit cell with lattice parameters $a = 2.08$ nm, $b = 1.64$ nm, and $\gamma = 93°$. The off-meridional reflections originate from a tilt of the discotic cores with respect to the columnar axis that is characteristic of the "herringbone" structure (C_r) as identified earlier [16].

The molecular dynamics of the disks involve different geometries as sketched in Fig. 3(e). In NMR, rotational motions are probed via second-rank tensors. The general expression for the angular dependent NMR frequency for an interaction λ is given by [17]

$$\omega_\lambda = \lambda_0 \tfrac{1}{2}(3\cos^2\alpha_\lambda - 1 - \eta_\lambda \sin^2\alpha_\lambda \cos 2\beta_\lambda). \quad (1)$$

The polar angles α_λ, β_λ describe the orientation of the magnetic field $\mathbf{B_0}$ in the principal axes system (PAS_λ) of the coupling, where we consider $^{13}\mathrm{C} - {}^1\mathrm{H}$ dipole-dipole coupling (DDC), $^2\mathrm{H}$ quadrupole coupling (QC), and $^{13}\mathrm{C}$ chemical-shift anisotropy (CSA). For fast molecular rotations with correlation times $\tau_c < 10^{-6}$ s that are characteristic of the Col_h phase, the interaction tensors are averaged. Nevertheless, the NMR frequencies can be described by an equation equivalent to Eq. (1):

$$\omega_{\lambda_a} = \lambda_a \tfrac{1}{2}(3\cos^2\alpha_{\lambda_a} - 1) \quad \text{and} \quad S_\lambda = \lambda_a/\lambda_0, \quad (2)$$

where a denotes "averaged." The maximum frequency shift (splitting) is found for $\mathbf{B_0}$ parallel to the unique axis of the PAS_λ, determined by λ_0 or λ_a The ratio of the motionally averaged and the static coupling parameters λ_a, and λ_0, respectively, defines the dynamic order parameter S_λ. Complex dynamics can lead to a sequence of averaged tensors, i.e., preaveraged by a first and further averaged by slower processes.

The fastest large amplitude core motion in DLCs is the local axial rotation of the disks, which leads to axially symmetric tensors with their unique axis along the normal to the disks ($\vec{n}$) [7,8,18]. The C-H bond directions probed via $^{13}\mathrm{C} - {}^1\mathrm{H}$ DDC or $^2\mathrm{H}$ QC lie in the plane of the disk and axial rotation reduces the coupling constant by a factor of 2, hence $S_{\mathrm{CH}} = 0.5$. For the $^{13}\mathrm{C}$ CSA of the aromatic core the unique axis is along $\vec{n}$ [17]. Therefore, local axial rotation only removes the in-plane anisotropy of the $^{13}\mathrm{C}$ CSA described by η_{CSA} and leaves the major component unaffected, hence $S_{\mathrm{CSA}} = 1.0$. In the Col_h phase, additional out-of-plane fluctuations and collective rotation around the column axis can occur, see Fig. 3(e), which further reduces the order parameters S_{CH} and S_{CSA}. In total, axially symmetric NMR coupling tensors result with their unique direction along the column axis $\vec{N}$.

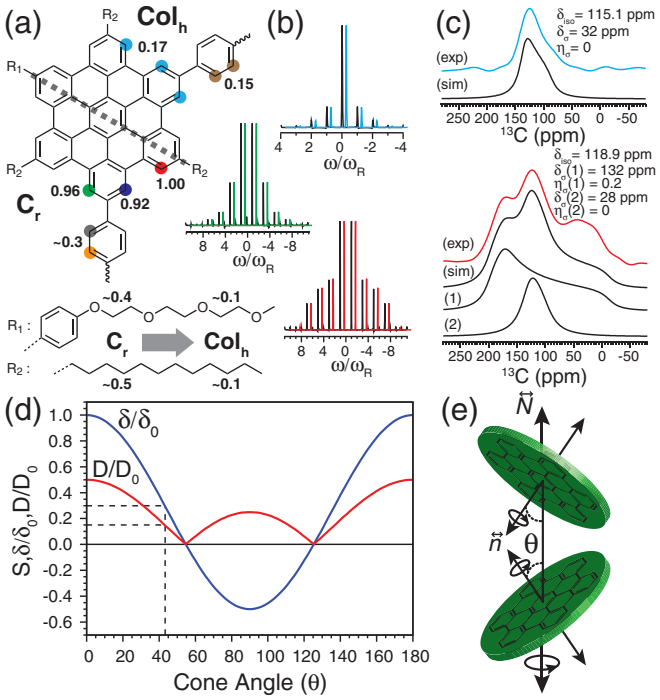

FIG. 3 (color). (a) Site-specific order parameters obtained from dipolar sideband patterns. Numbers above and below the dashed line correspond to order parameters in the Col_h (378 K) and C_r (315 K) phases, respectively. (b) Representative examples of $^{13}\mathrm{C} - {}^1\mathrm{H}$ dipolar sideband patterns. The simulated sideband patterns were obtained using a two-component fit [18,26]. (c) Quasistatic $^{13}\mathrm{C}$ CSA powder patterns recorded in the Col_h (top) and C_r phases (bottom) using the SUPER experiment [20]. The simulated spectra in the C_r phase include two components characteristic of (1) frozen and (2) mobile disks undergoing the type of motion illustrated in (e). (d) Twofold motional averaging of the anisotropic $^{13}\mathrm{C} - {}^1\mathrm{H}$ DDC and $^{13}\mathrm{C}$ CSA tensor components as a result of fast axial rotation combined with an n-site jump scenario ($n \geq 3$) as illustrated in (e).

In order to probe these dynamics, solid-state NMR spectra were recorded using the $^{13}\mathrm{C} - {}^1\mathrm{H}$ rotor-encoded rotational echo double-resonance (REREDOR) and rotor-encoded polarization transfer heteronuclear dipolar order (REPT-HDOR) techniques [19]. These experiments employed spinning frequencies, ν_R, of 29.762 kHz (REPT-HDOR, 134.4 μs recoupling time) and 25.0 kHz (REREDOR, 240.0 μs recoupling time) at temperatures $T = 315$ and 378 K, respectively, and yield site-specific $^{13}\mathrm{C} - {}^1\mathrm{H}$ DDCs. The quasistatic $^{13}\mathrm{C}$ CSA powder patterns were recorded using separation of undistorted powder patterns by effortless recoupling (SUPER) [20] experiments using $\nu_R = 5.0$ kHz for $T = 285$ and 365 K. Experiments were performed on Bruker DSX 300 (SUPER) and Bruker Avance-III 850 (REREDOR/REPT-HDOR) spectrometers using double-resonance magic-angle spinning (MAS) probes with 2.5 mm rotors. The principal elements of the DDC (D) and CSA (δ) tensors are ordered according to the conventions given in [17].

In the C_r phase, the values for S_{CH} of the HBC core [Fig. 3(b)] indicate a frozen column in agreement with the WAXS results. Yet, the side chains display restricted dynamics with $S_{\mathrm{CH}} \sim 0.4$–0.5 which is also detected in DS. In

the Col_h phase, however, S_{CH} for the HBC core is dramatically decreased down to ~0.15, suggesting a highly disordered columnar structure.

In the heterogeneous scenario [Fig. 1(b), right] as deduced from WAXS above, collective columnar rotation of the stacks inclined at an angle θ to the column axis is expected [Fig. 3(e)]. For both the preaveraged $^{13}C - {}^{1}H$ DDC and ^{13}C CSA interactions, the effect of an additional fast motion can simply be modeled by a jump motion with threefold or higher symmetry on a cone with opening angle θ [21]. In Fig. 3(d) the dependence of S_{CH} and S_{CSA} on the angle θ is plotted. The latter exhibits the characteristic $P_2(\cos\theta)$ behavior of second-rank tensors with axial symmetry, where S_{CSA} is positive for $0° \leq \theta \leq 54.7°$ and negative for $54.7° \leq \theta \leq 90°$. The asymmetric ^{13}C CSA powder line shape reveals this kind of information, while the sign is lost in the symmetric spectra due to $^{13}C - {}^{1}H$ DDCs. Moreover, the absolute values of S_{CH} and S_{CSA} differ by a factor of 2, because of the preaveraging noted above. Taking this into account, the absolute values for S_{CH} and S_{CSA} of ~0.15 and ~0.27, respectively, describe the same packing and from the ^{13}C CSA powder line shape [Fig. 3(c)], S_{CSA} is positive. Therefore, the cone angle can be deduced to be $\theta \sim 43°$ as indicated in Fig. 3(d). In the Col_h phase it is highly likely that in addition to the collective rotation of the stacks around the column axis, intracolumnar exchange of disks between stacks or even flipping of whole stacks from $+\theta$ to $-\theta$ will occur, see Fig. 1(c). However, due to the second-rank tensor character, $\pm\theta$ cannot be distinguished and such exchange processes are not detected by the NMR techniques employed here.

Our NMR data can thus be quantitatively analyzed in terms of heterogeneous disorder [Fig. 1(b), right] with highly ordered stacks of limited length inclined at angles $\pm\theta$. For space filling reasons the columns must in addition contain disordered and, hence, more mobile regions between the stacks. Indeed, in the solid C_r phase, the ^{13}C CSA powder line shape, Fig. 3(c), contains a narrow component (~ 20%–25%) in addition to the broad pattern representative of the frozen stacks. This mobile fraction also shows up in Fig. 3(b), where it contributes to the inner DDC sidebands [18]. Thus, the system studied here displays regions of vastly different order and mobility demonstrating that the columns include a considerable fraction of defects.

Rheology follows the viscoelasticity in the two phases and is sensitive to slower dynamics. Figure 4 shows the storage and loss moduli on cooling in isochronal conditions ($\omega = 10$ rad/s). A significant increase of both moduli on cooling at ~315 K is observed indicating the formation of the solid phase. The difference in the viscoelastic properties of the two phases can be probed by isothermal frequency sweeps at selected temperatures, corresponding to the C_r and Col_h phases (Fig. 4). The C_r phase has an elastic

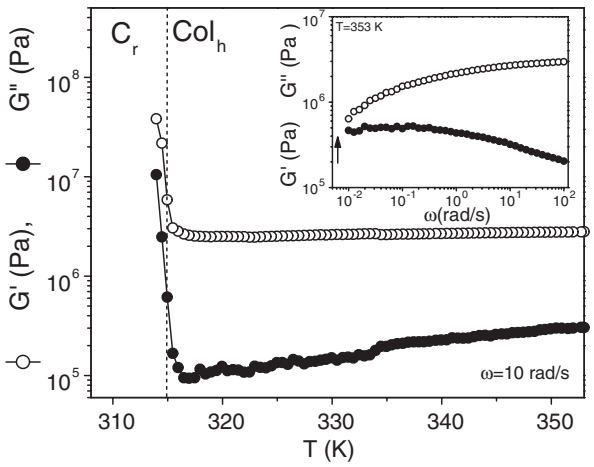

FIG. 4. Temperature dependence of the storage (open circles) and loss (filled circles) moduli obtained at 10 rad/s on cooling with 2 K/min. The vertical lines indicate the Col_h to C_r transition temperature. (Inset): Frequency dependence of the storage (open circles) and loss (filled circles) moduli $T = 353$ K, corresponding to the Col_h phase. The arrow gives the characteristic frequency corresponding to the expected crossing of the storage and loss moduli.

response ($G' \sim \omega^0$, $G'' \sim \omega^0$) [14], suggesting a strong influence of the rigid columnar segments, whereas the Col_h phase ($T = 353$ K) has a viscoelastic character. In addition, the storage modulus G' and the characteristic frequency ω_c (arrow in Fig. 3) can be used to obtain a characteristic length $d \approx 2.1$ nm of the defect texture of the unaligned HBC, as $G' \sim k_B T/d^3(\omega_c\tau)^2$ [22,23]. Considering the intracolumnar periodicity within the Col_h phase this length corresponds to about seven disks in excellent agreement with the results from WAXS. The associated timescale is $\sim 7 \times 10^2$ s indicating a very slow cooperative defect diffusion within the Col_h phase most likely due to intercolumnar exchange [Fig. 1(d)].

To conclude, the heterogeneous disorder of the disks found here can be viewed as an extreme case of the packing problem pointed out by de Gennes [5] and also found in recent MD simulations [24,25]. To the best of our knowledge, such a combination of highly ordered local stacks and regions of high dynamic disorder in a DLC, leading to nanostructured columns, has not been found and quantified experimentally before. However, the LC phase of HBCs appears to be extremely stable towards the presence of such defects accommodating order parameters as low as 0.3 for the disk normal. The characteristic length scale associated with the stacks is 7–8 disks, severely limiting the long-range charge transport [6]. Complex dynamics differing by at least 8 orders of magnitude have been observed and were assigned to intra- and intercolumnar processes.

This work was supported by the DFG (SFB 625), by the Greek Ministry of Education (HRAKLEITOS II) and the

region of Epirus (Research unit on Dynamics and Thermodynamics of the UoI co-financed by the European Union and the Greek state under NSRF 2007-2013). Discussions with Dr. R. Graf, Dr. D. Andrienko, and Professor K. Kremer are gratefully acknowledged.

*Corresponding author.
mrh@mpip-mainz.mpg.de
†Corresponding author.
gfloudas@cc.uoi.gr

[1] C. K. Ober *et al.*, Macromolecules **42**, 465 (2009).
[2] L. Schmidt-Mende *et al.*, Science **293**, 1119 (2001).
[3] A. P. H. J. Schenning and E. W. Meijer, Chem. Commun. (Cambridge), 26 (2005) 3245.
[4] J. Wu, W. Pisula, and K. Müllen, Chem. Rev. **107**, 718 (2007).
[5] P. G. DeGennes, J. Phys. (Paris), Lett. **44**, 657 (1983).
[6] P. W. Anderson, Phys. Rev. **109**, 1492 (1958).
[7] M. M. Elmahdy *et al.*, Phys. Rev. Lett. **100**, 107801 (2008).
[8] A. Fechtenkötter *et al.*, Angew. Chem., Int. Ed. **38**, 3039 (1999).
[9] M. M. Elmahdy *et al.*, J. Am. Chem. Soc. **130**, 5311 (2008).
[10] X. Feng *et al.*, J. Am. Chem. Soc. **131**, 4439 (2009).
[11] E. Fontes *et al.*, Phys. Rev. A **37**, 1329 (1988).
[12] A. Levelut, J. Phys. (Paris), Lett. **40**, L81 (1979).
[13] C. R. Safinya *et al.*, Phys. Rev. Lett. **53**, 1172 (1984).
[14] C. Grigoriadis *et al.*, Soft Matter **7**, 4680 (2011).
[15] E. Fontes, P. A. Heiney, and W. H. de Jeu, Phys. Rev. Lett. **61**, 1202 (1988).
[16] C. Ochsenfeld *et al.*, J. Am. Chem. Soc. **123**, 2597 (2001).
[17] K. Schmidt-Rohr and H. W. Spiess, *Multidimensional Solid-State NMR and Polymers* (Academic, New York, 1994).
[18] M. R. Hansen *et al.*, Angew. Chem., Int. Ed. **48**, 4621 (2009).
[19] K. Saalwächter and I. Schnell, Solid State Nucl. Magn. Reson. **22**, 154 (2002).
[20] S. F. Liu, J. D. Mao, and K. Schmidt-Rohr, J. Magn. Reson. **155**, 15 (2002).
[21] V. Macho, L. Brombacher, and H. W. Spiess, Appl. Magn. Reson. **20**, 405 (2001).
[22] R. G. Larson *et al.*, Rheol. Acta **32**, 245 (1993).
[23] R. H. Colby *et al.*, Rheol. Acta **36**, 498 (1997).
[24] J. Kirkpatrick *et al.*, Phys. Rev. Lett. **98**, 227402 (2007).
[25] V. Marcon *et al.*, J. Chem. Phys. **129**, 094505 (2008).
[26] M. Bak, J. T. Rasmussen, and N. C. Nielsen, J. Magn. Reson. **147**, 296 (2000).